THE APOLLONIAN DECAY OF BEER FOAM BUBBLE SIZE DISTRIBUTION AND THE LATTICES OF YOUNG DIAGRAMS AND THEIR CORRELATED MIXING FUNCTIONS

S. SAUERBREI, E. C. Haß, AND P. J. PLATH

Received 4 August 2005; Accepted 3 October 2005

We present different methods to characterise the decay of beer foam by measuring the foam heights and recording foam images as a function of time. It turns out that the foam decay does not follow a simple exponential law but a higher-order equation $\ln V(t) = a - bt - ct^{2.5}$, which can be explained as a superposition of two processes, that is, drainage and bubble rearrangement. The reorganisation of bubbles leads to the structure of an *Apollonian gasket* with a fractal dimension of $D \approx 1.3058$. Starting from foam images, we study the temporal development of bubble size distributions and give a model for the evolution towards the equilibrium state based upon the idea of Ernst Ruch to describe irreversible processes by lattices of *Young diagrams*. These lattices generally involve a partial order, but one can force a total order by mapping the diagrams onto the interval $[0,1]$ using ordering functions such as the *Shannon entropy*. Several *entropy-like* and *nonentropy-like mixing functions* are discussed in comparison with the *Young order*, each of them giving a special prejudice for understanding the process of structure formation during beer foam decay.

1. Introduction

Beer foam is a fascinating subject not only for connoisseurs of selected cultivated beers but for scientists as well. Some years ago, in 2002, Leike [14] published his observations on the decay of beer froth. He found that the volume of beer froth decays exponentially with time. He looked for the height of the froth for different kinds of German beer as a function of time. His best fits represent the decay only in the beginning. However, Dale et al. have already published their fundamental results on the decay of beer foam in 1993 [8]. They investigated the temporal change in the conductivity of the collapsing beer foam. They distinguished between three decay phases—the initial phase I, the consolidation phase C, and the residual R. For the first two phases I and C they estimated simple exponential laws for the decay of the foam mass. They concluded that at the first

Hindawi Publishing Corporation
Discrete Dynamics in Nature and Society
Volume 2006, Article ID 79717, Pages 1–35
DOI 10.1155/DDNS/2006/79717

stage *I* of foam collapse the liquid beer drainage driven by gravity is the most important process. This process takes about 300 seconds. The consolidation stage *C* is characterised by an increase of the concentration of polypeptide material in the foam. The enrichment of surface active molecules in the bubble lamella—leading, for example, to bubble coalescence—is responsible for the collapse process.

Following these arguments, one may call in question the results presented by Leike [14]. This leads to the problem, if it is possible to find a similar separation of different processes in the temporal development of the foam volume. Usually one describes foams by their bubble or cavity size distribution function. How does the bubble size distribution function develop during the decay of the foam? No answers, neither for beer foam, nor for other fast collapsing fluid/gas foams, are known to this question. The problem is that one cannot simply look into the three-dimensional body of the foam because of the refraction of light.

Especially in case of beer foam it is well known that the surface of the beer glass strongly influences the properties of the foam. Therefore, it seems to be very hard to conclude to the inner bubble size distribution function from looking at the outside of the glass. Nevertheless, there should be at least some correlations between the outer and the inner structure of the bubble arrangement, which could be figured out by looking at the temporal development of the foam as well as of the increase of the liquid beer flowing out of the foam. It is our aim to get information about the structure of the body of the foam by looking only from the outside.

2. Experimental setup

In order to investigate the decay of beer foam, at first one has to produce the foam. The traditional way of producing beer foam is to pour a glass of beer. Unfortunately, this method does not lead to reproducible results, since one cannot reproduce the initial bubble size distribution function. For this reason, we decided to foam up the *unfoamed beer* with ultrasound (Ultrasonik 28x; NEY) for 13 seconds. This *unfoamed beer* is allowed only to posses at most 5% of foam with respect to its fluid part.

It is well known that the shape of the glass and the amount of beer to be foamed will influence the decay of the beer foam. For this reason we investigated the decay of the foam in different measuring glasses (100 ml, 2.6 cm in diameter; 250 ml, 3.6 cm in diameter; and 500 ml, 5 cm in diameter) with different amounts of beer: 20 ml beer in the 100 ml measuring glass (abbreviation: 20/100), 50 ml beer in the 250 ml glass (50/250), and 100 ml beer in the 500 ml measuring glass (100/500). To investigate the temperature influence on the decay of foam, we used different temperatures in our beer foam experiments: $T = 0^\circ \pm 1^\circ$ C, $8^\circ \pm 1^\circ$ C, and $24^\circ \pm 1^\circ$ C.

Using these experimental conditions, the initial volume at time $t_0 = 0$ of the freshly generated foam after ultrasound treatment was about twice as much compared to the volume of the unfoamed beer. About 10 Vol.%—with respect to the foam volume—of the beer remained unfoamed. For example, in case of 20 ml beer we obtained 40 ml foam and 4 ml unfoamed beer after ultrasound foaming.

The volume of the foam and the liquid beer phase was measured in time intervals of 20 seconds by visual inspection.

In order to estimate the bubble size distribution function, we analysed photographs of collapsing beer foam by an optical measuring technique and computer-aided image processing [10]. The measuring device consisted of a high resolution CCD-camera (JAI CV-A11), a telecentric lens, coaxial diffuse illumination, and a fast frame grabber card, leading to an accuracy up to 5 μm. The photographs were recorded every five seconds starting one minute after foaming up. In order to avoid optical distortions, the beer foam was generated in special square glass vessels (2.5×2.5 cm) manufactured in our laboratories.

3. Results

3.1. Temporal behaviour of the foam volume. We investigated the volume dependence $V(t)$ of beer foam decay measuring the height of the foam and the level of liquid beer as a function of time. In every case we averaged arithmetically five independent measurements under the same conditions. The data obtained were approximated by various curve fitting calculations. Out of the tested fitting functions we always found the following fitting formula $V(t)$ with highest priority:

$$\ln V(t) = a - bt - ct^{2.5} \tag{3.1}$$

fulfilling the constraints

$$\lim_{t\to\infty} V(t) = 0, \quad V(t) \geq 0 \quad \forall\, t > t_0. \tag{3.2}$$

Using (3.1), we estimated the coefficients for many kinds of beer and different temperatures in different glasses.

Taking *Beck's Pils* from Bremen, for instance, we obtained in case of the (20/100/24° C) experiment equation (3.3) (see Figure 3.1):

$$\begin{aligned} V(t) &= \exp(a)\exp(-bt)\exp\left(-ct^{2.5}\right), \\ \ln V(t) &= 3.64 - 4.34 \cdot 10^{-3} t - 6.66 \cdot 10^{-7} t^{2.5}, \qquad R^2 = 0.998. \end{aligned} \tag{3.3}$$

This is not an ordinary (simple) exponential function, but it can be interpreted as a product function decomposable into two separate functions, which describe different processes of the foam decay at different time intervals:

$$\begin{aligned} V_1(t) &= \exp\left(a_1\right)\exp\left(-b_1 t\right), \\ \ln V_1(t) &= a_1 - b_1 t, \\ \ln V_1(t) &= 3.66 - 5.40 \cdot 10^{-3} t \end{aligned} \tag{3.4}$$

for $0\,\text{s} \leq t \leq 160\,\text{s}$, and

$$\begin{aligned} V_2(t) &= \exp\left(a_2\right)\exp\left(-c_2 t^{2.5}\right), \\ \ln V_2(t) &= a_2 - c_2 t^{2.5}, \\ \ln V_2(t) &= 3.02 - 1.13 \cdot 10^{-6} t^{2.5} \end{aligned} \tag{3.5}$$

for $200\,\text{s} \leq t \leq 380\,\text{s}$.

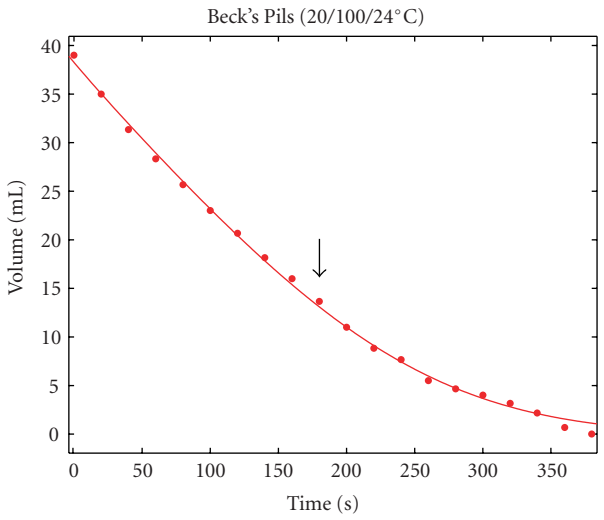

Figure 3.1. The volume of the beer foam as a function of time. The fitting function is given by (3.3). The arrow approximately indicates the point, where drainage switches to bubble rearrangement as dominating process.

The coefficient $a \approx a_1$ represents the foam volume $V(0) \equiv V_0$; $V_1(0) = \exp(a_1) \approx \exp(a) = V_0$ immediately after the ultrasound foaming up of the beer. b_1 is the coefficient of the exponential decay at the beginning, which is mainly caused by the drainage of the liquid beer out of the foam (see Figure 3.2). The essential new factor is the term $-c_2 t^{2.5}$ or $\exp(-c_2 t^{2.5})$, respectively. The corresponding function $V_2(t) = \exp(a_2)\exp(-c_2 t^{2.5})$—which has never been described before—represents the rearrangement of the bubbles in the second time interval C (see Figure 3.2). The coefficient a_2 represents the fictive volume $V_2(0) = \exp(a_2)$ of this second process at $t_0 = 0$. The character of this process will be discussed later.

The temperature dependence is shown in Table 3.1 for *Beck's Pils* in the (20/100) experiments. The lower the temperature is the smaller the amount of initial foam volume $V_0 = \exp(a)$ in $\ln V(t)$ after ultrasound treatment of beer is and the faster the drainage is. This can be seen from the coefficients b and b_1, respectively. The coefficients of the rearrangement process in the phase C decrease with lowering the temperature, which indicates a slowing down of the underlying process of bubble rearrangement.

Table 3.2 shows an example of the influence of the size of the beer glass on the decay of beer foam.

Taking wider glasses, we needed more beer for inspection of the decay of foam. The wider the glasses are and the more beer has to be foamed up, the slower the drainage is and the rearrangement processes are in tendency. For wider glasses it is much more difficult to separate the two processes (see Figure 3.3).

Comparing different kinds of beer at the standard experimental conditions (20/100/24), Table 3.3, we obtained the coefficients shown in Table 3.3. As can be seen, in case of

Table 3.1. Temperature dependence of the coefficients for *Beck's Pils* in the (20/100) experiments.

Beck's Pils	$a/a_1/a_2$	b/b_1	c/c_2
20/100/0° C			
$\ln V(t)$	3.42	$4.83 \cdot 10^{-3}$	$3.22 \cdot 10^{-7}$
$\ln V_1(t)$	3.43	$5.65 \cdot 10^{-3}$	—
$\ln V_2(t)$	2.85	—	$9.12 \cdot 10^{-7}$
20/100/8° C			
$\ln V(t)$	3.56	$4.56 \cdot 10^{-3}$	$4.48 \cdot 10^{-7}$
$\ln V_1(t)$	3.58	$5.53 \cdot 10^{-3}$	—
$\ln V_2(t)$	3.03	—	$1.01 \cdot 10^{-6}$
20/100/24° C			
$\ln V(t)$	3.64	$4.34 \cdot 10^{-3}$	$6.66 \cdot 10^{-7}$
$\ln V_1(t)$	3.66	$5.40 \cdot 10^{-3}$	—
$\ln V_2(t)$	3.02	—	$1.13 \cdot 10^{-6}$

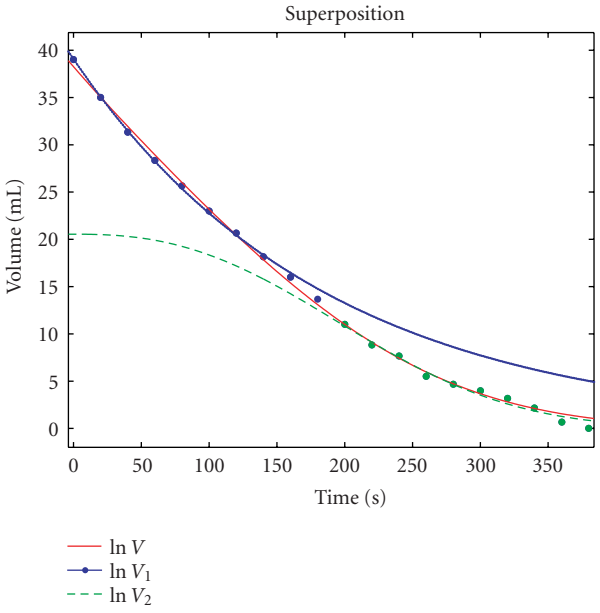

Figure 3.2. The foam volume as a function of time. The three different functions $\ln V$, $\ln V_1$, and $\ln V_2$ are put together in this figure for comparison.

Diebel's Alt one gets more foam and the lowest decay by drainage and during rearrangement. In other words, under these conditions the foam of *Diebel's Alt* is more stable than that of *Beck's* or *Vitamals*.

It seems to be possible to enhance such kinds of measurements in order to compare the foam quality of different kinds of beer.

Table 3.2. Influence of the size of the beer glass on the decay of the beer foam (*Beck's Alkoholfrei*) at 24° C.

Beck's Alkoholfrei	$a/a_1/a_2$	$V_0/V_1/V_2$ (mL)	b/b_1	c/c_2
20/100/24° C				
$\ln V(t)$	3.64	38.09	$4.34 \cdot 10^{-3}$	$6.66 \cdot 10^{-7}$
$\ln V_1(t)$	3.66	38.86	$5.40 \cdot 10^{-3}$	—
$\ln V_2(t)$	3.02	20.49	—	$1.13 \cdot 10^{-6}$
50/250/24° C				
$\ln V(t)$	4.65	104.58	$2.67 \cdot 10^{-3}$	$4.64 \cdot 10^{-7}$
$\ln V_1(t)$	4.68	107.77	$3.89 \cdot 10^{-3}$	—
$\ln V_2(t)$	4.24	72.24	—	$6.74 \cdot 10^{-7}$
100/500/24° C				
$\ln V(t)$	5.27	194.42	$2.92 \cdot 10^{-3}$	$3.94 \cdot 10^{-7}$
$\ln V_1(t)$	5.30	200.34	$3.90 \cdot 10^{-3}$	—
$\ln V_2(t)$	4.68	129.02	—	$6.70 \cdot 10^{-7}$

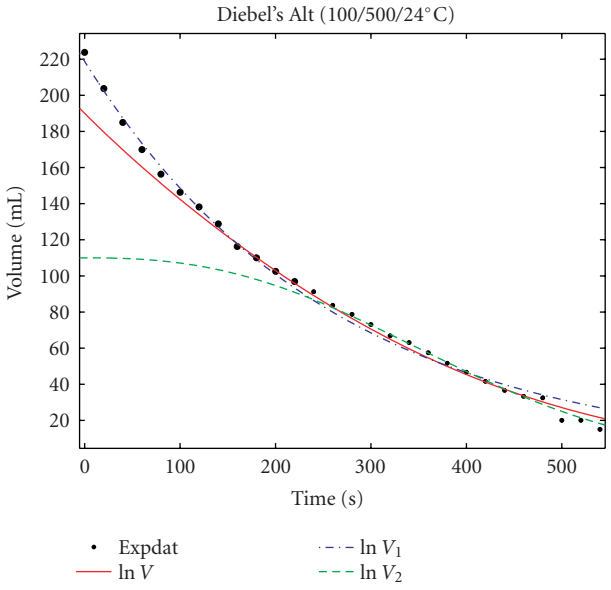

Figure 3.3. An example for the decay of beer foam which is not separable under these conditions.

3.2. Drainage process. Dale et al. suggested that the exponential shrinking of the volume according to (3.4) is mainly caused by the drainage [8]. A first inspection seems to support this idea, since the fitting curve $V_1(t) = \exp(a_1)\exp(-b_1 t)$ for the data of the initial phase I ($0\,\mathrm{s} \le t \le 160\,\mathrm{s}$) is an exponential one.

Table 3.3. Comparison of beer foam decay for different kinds of beer under the same constraints of the 20/100/24° C experiments.

	$a/a_1/a_2$	$V_0/V_1/V_2$ (mL)	b/b_1	c/c_2
Beck's Pils 20/100/24° C				
$\ln V(t)$	3.64	38.09	$4.34 \cdot 10^{-3}$	$6.66 \cdot 10^{-7}$
$\ln V_1(t)$	3.66	38.86	$5.40 \cdot 10^{-3}$	—
$\ln V_2(t)$	3.02	20.49	—	$1.13 \cdot 10^{-6}$
Diebel's Alt 20/100/24° C				
$\ln V(t)$	3.83	—	$4.06 \cdot 10^{-3}$	$5.25 \cdot 10^{-7}$
$\ln V_1(t)$	3.85	—	$5.10 \cdot 10^{-3}$	—
$\ln V_2(t)$	3.38	—	—	$1.06 \cdot 10^{-6}$
Vitamals 100/100/24° C				
$\ln V(t)$	3.66	—	$5.46 \cdot 10^{-3}$	$6.54 \cdot 10^{-7}$
$\ln V_1(t)$	3.67	—	$6.42 \cdot 10^{-3}$	—
$\ln V_2(t)$	3.10	—	—	$1.50 \cdot 10^{-6}$

However, this drainage process is at the same time overlaid by the beginning of the rearrangement. Possibly, the separation into two parts of the overall function (3.3) based on the experimental data enables studying the underlying processes in more detail.

In the region between 200 s and 380 s the function of the temporal dependence of the volume has been determined to be $V_2(t) = \exp(a_2)\exp(-c_2 t^{2.5})$ (3.5), where $V_{2,0} \equiv V_2(0)$ is the fictitious initial volume for this process of bubble rearrangement. If we calculate the difference between the experimental data in the first time interval I and the function $V_2(t)$, we can estimate the function of the pure drainage without the contribution of the rearrangement process by

$$V_d \approx V(t) - V_2(t) \tag{3.6}$$

for $0\,\text{s} \le t \le 160\,\text{s}$.

The best fit for these data is the following parabola (see Table 3.4 and Figure 3.4):

$$V_d = \frac{a + ct + et^2}{1 + bt + dt^2}, \qquad R^2 = 0.999998. \tag{3.7}$$

Even simpler parabola will give reasonable results like, for example,

$$V_d = a + bt + ct^2, \qquad R^2 = 0.9999, \tag{3.8}$$

or

$$V_d = a + bt + ct^{2.5}, \qquad R^2 = 0.9988, \tag{3.9}$$

Table 3.4. Coefficients of (3.7) for the drainage process.

$a = 17.54$	$b = 3.8 \cdot 10^{-4}$	$c = -1.5 \cdot 10^{-1}$	$d = 1.05 \cdot 10^{-5}$	$e = 3.43 \cdot 10^{-4}$

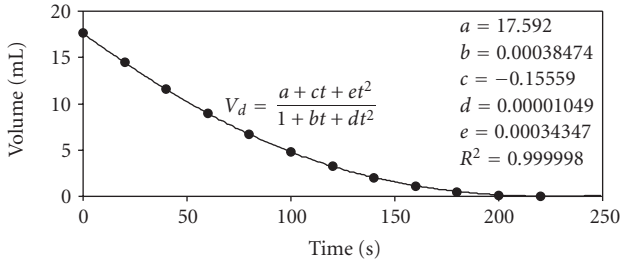

Figure 3.4. Fitting of the drainage data by the function of (3.7).

however, all these fitting functions do not fulfil the (artificial) constraint $\lim_{t\to\infty} V_d(t) = 0$, which means that the experimental data are embedded in the function $V_2(t)$ for the interval $200 \le t \le \infty$, unless a third process starts to govern the decay of the foam at time $t \ge 330\,\text{s}$.

An exponential approach of the type

$$V_d = a + b \exp \frac{-t}{c}, \qquad R^2 = 0.9975, \tag{3.10}$$

exhibits systematic deviations from the experimental data. So, the above-mentioned parabola (3.7) is the best description for the experimentally observed temporal decay of the foam volume, if one considers drainage as its only reason. For the moment we are far from understanding this process. Therefore, we have to restrict ourselves presently only on experimental data and first numerical results of the very complex behaviour of the foam decay by drainage.

3.3. The Apollonian rearrangement. The temporal behaviour of the bubble rearrangement in the consolidation stage C ($200\,\text{s} < t < 380\,\text{s}$) is described in a very good agreement by the equation $V_2(t) = \exp(a_2)\exp(-c_2 t^{2.5})$ (3.5).

Dale et al. assumed that the increase of the concentration of polypeptide materials in the foam lamella is responsible for this consolidation [8]. We observed a dramatic change in the bubble size distribution function, which starts from a very sharp distribution function of very small bubbles just after ultrasound foaming up. Simple visual inspections of the changes in the foam during this time interval indicate that the bubble rearrangement is the essential process. Within time, large bubbles survive surrounded by small and very small bubbles, which are filling the remaining spacing between the larger bubbles (Figure 3.5). These structures are strongly suggestive for the structure of an *Apollonian gasket* (Figure 3.8).

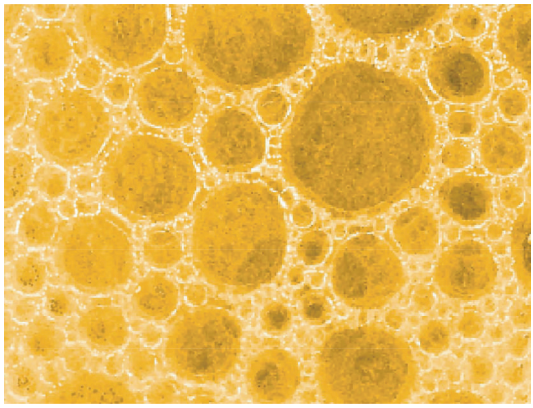

Figure 3.5. *Apollonian foam* at the inner walls of a plane beer glass.

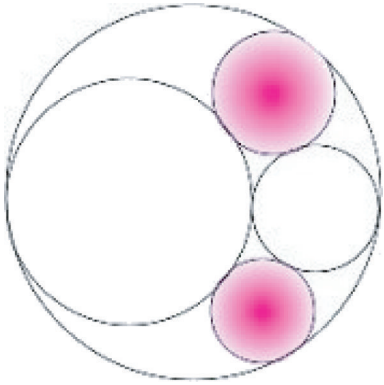

Figure 3.6. The construction of Apollonios of Perge (see [17]).

Apollonios of Perge (262 to 192 BC [28]) put two circles (of different sizes) inside a large one, both touching each other and the large one at three different points of contact (see Figure 3.6). In both the two remaining circular triangles he inscribed the largest possible circles (called *Apollonian circles,* represented with magenta colour in Figure 3.6), each of them having contact with the original circles at three points. He ended up with five circles and six spacing circular triangles [17].

G. W. Leibniz (1646–1716) [17] repeated this procedure ad infinitum (compare Figure 3.7):

> Imagine a circle; inscribe within three other circles congruent to each other, and of maximum radius; proceed similarly with each of these circles and within each interval between them, and imagine that the process continues to infinity … (quoted from Mandelbrot, *The Fractal Geometry of Nature*, page 170) [15, 16].

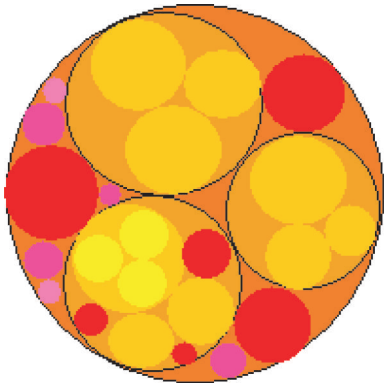

Figure 3.7. Sketch of the Leibniz packing.

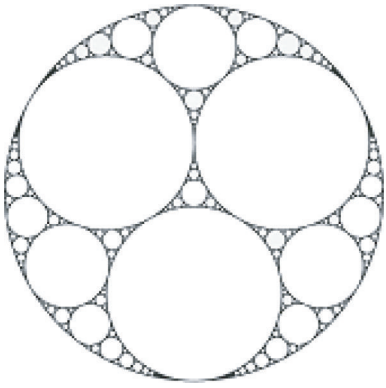

Figure 3.8. Apollonian gasket.

His construction is known today as the *Apollonian packing* or *Leibniz packing* [16]. Following the notation of Mandelbrot, a finite set of Apollonian circles constructed this way is called *Apollonian gasket* (Figure 3.8).

The Apollonian cascade is not self-affine. Nevertheless, one can use the Hausdorff-Besicovitch definition to define a measure. Boyd [3, 4] has estimated numerically this fractal dimension D to be in the range of

$$1.30197 < D < 1.314534 \quad [4], \qquad \text{or} \qquad D \approx 1.3058 \quad [3]. \tag{3.11}$$

In order to confirm the assumption that the bubble rearrangement during the consolidation phase C is just the formation of an Apollonian gasket, we estimated the Hausdorff-Besicovitch dimension D for the photographs, which have been taken from the bubbles on the walls inside the beer glasses. For this purpose we used a special square glass vessel in order to get plane surfaces.

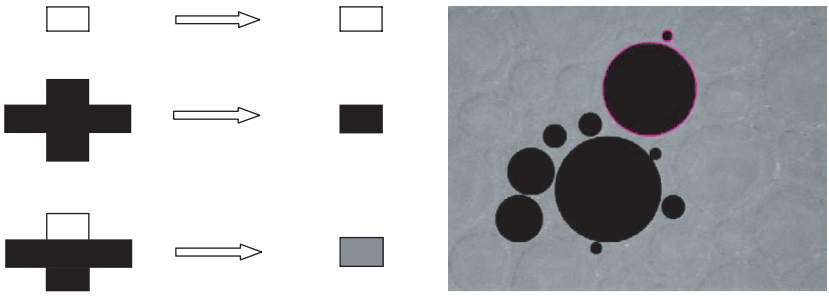

Figure 3.9. Cellular automata are used to estimate the borderlines of the black disks representing the bubbles in the foam: (a) transformation rules of the cellular automaton, (b) black disks and surrounding borderlines (pink coloured), exemplarily drawn for two bubbles.

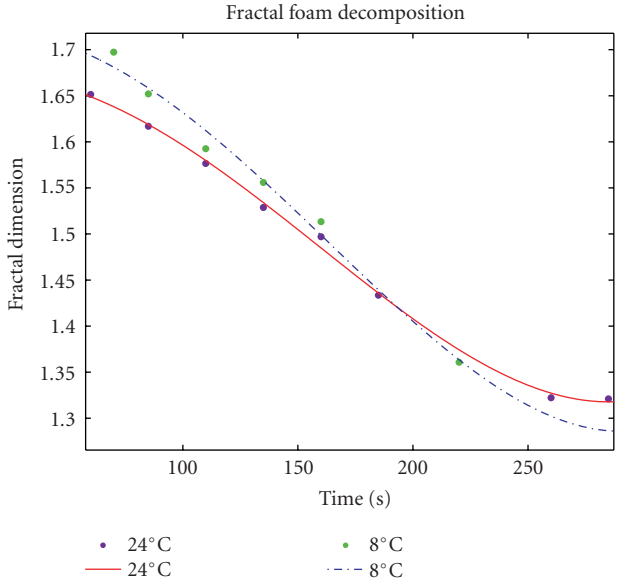

Figure 3.10. The fractal dimension D as function of time for the decomposition of the foam of *Beck's Alkoholfrei* beer at various temperatures. The spline functions are given by (3.12).

The grey valued pictures of the bubbles have to be transformed firstly into binary pictures (black and white pictures). Using cellular automata we estimated the borderlines of the black disks getting a set of circles (see Figure 3.9).

From these pictures of the borderlines we calculated the fractal dimensions D of the arrangement of circles at different times. The dimension D of the set of circles converges to the dimension of the Apollonian gasket (Figure 3.10).

Table 3.5. Coefficients of (3.12).

Beck's Alkoholfrei	a_D	b_D	c_D	d_D	R^2
8° C	1.72	$1.00 \cdot 10^{-5}$	$1.84 \cdot 10^{-6}$	$9.01 \cdot 10^{-8}$	0.987
24° C	1.67	$1.24 \cdot 10^{-5}$	$1.56 \cdot 10^{-6}$	$7.77 \cdot 10^{-8}$	0.997

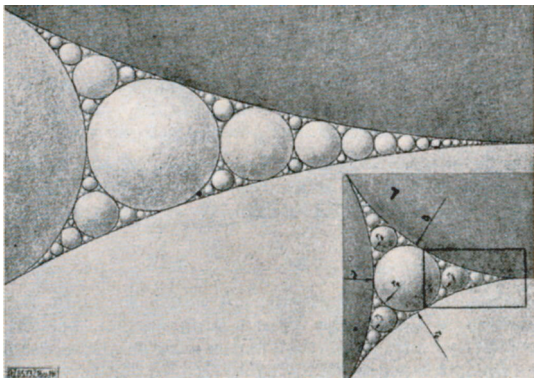

Figure 3.11. Apollonian spheres (this reproduction has been taken from [18]; the publishing house does not exist any more).

In order to quantify the statement of the temporal behaviour of the fractal dimension D, we estimated the spline functions (3.12) (see Figure 3.10):

$$D(t) = a_D - b_D t - c_D t^{2.5} + d_D t^3 \tag{3.12}$$

for the decay of the foam volume at 8° C and 24° C in case of *Beck's Alkoholfrei* beer (see Figure 3.10 and Table 3.5 for the temperature dependence of the coefficients).

It is an interesting result that one can correlate the fractal dimension D of the pictures of the foam surfaces with the state of the decomposition of the foam. As a consequence, one can state that the fractal Hausdorff-Besicovitch dimension D of these pictures is a measure for the geometrical rearrangement process of the foam bubbles.

One may argue that one cannot conclude from the inspection of the outer surface of the foam to its inner part. Therefore it should not be allowed to extrapolate the Apollonian rearrangement observed on the foam surface to the processes in the interior of foam. On the other hand, there is an early work on Apollonian packages of spheres [7, 18], which has already been used to describe dense mixtures of particles of very different sizes (Figure 3.11). Moreover, Japanese mathematicians of the Wasan school discussed in 1822 a similar problem on wooden *Sangaku Tables* in order to put *Kissing Spheres* inside a sphere [20, 22].

Sometimes, one can even recognise bubbles belonging somehow to the inner part of the foam and one can detect a structure, which resembles strongly an Apollonian gasket of spheres. This is by no means a proof, but it is a strong indication that the rearrangement

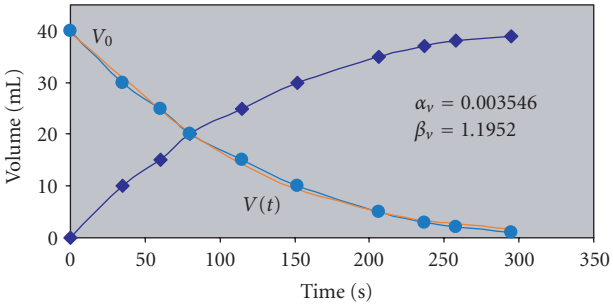

Figure 3.12. Time dependence of the volume of the liquid beer phase flowing out of the foam (dark blue), the portion of fluid beer in the foam (blue) and fitted curve (red).

of foam bubbles as an Apollonian package of spheres occurs in the interior of foam in a similar way as compared to the interface area of the foam and the glass wall.

3.4. The liquid content of the foam. In brewery techniques it is important to know the amount of liquid phase in the foam at time t. Obviously, one can record the increasing volume of fluid beer under the foam (see Figure 3.12) getting also the remaining portion of the liquid phase in the foam [2].

The time-dependence of the liquid volume fraction in the foam is given by

$$V(t) = V_0 \exp\left(-\alpha_V t^{\beta_V}\right), \qquad V_0 = V_{\text{total}}, \qquad \lim_{t\to\infty} V(t) = 0, \tag{3.13}$$

where α_V and β_V are the coefficients of the corresponding regression curve ($\beta_V \approx 1$).

On the other hand, from the recorded photographs (Figure 3.13) one can estimate the size of the bubble area $A_B(t)$ which covers the foam picture at time t. Referring to the total image area A_I, one can calculate the remaining non-bubble area $A_L(t)$ which represents the liquid part of the two-dimensional foam image (3.14),

$$\begin{gathered} A_L(t) = (A_I - A_B(t)) = (A_I - A_B(0)) \exp\left(-\alpha_A t^{\beta_A}\right), \\ (A_I - A_B(0)) \propto V_{\text{total}}, \\ \lim_{t\to\infty} A_L(t) = \lim_{t\to\infty} (A_I - A_B(t)) = 0, \\ \alpha_A,\ \beta_A = \text{coefficients of the regression curve } (\beta_A \approx 2). \end{gathered} \tag{3.14}$$

Figure 3.14 shows the temporal development of the *two-dimensional liquid area* of the images and Figure 3.15 a snapshot of the bubbles after 165 seconds.

Now, one can correlate the liquid volume $V(t)$ (see Figure 3.12) of the three dimensional foam and the *two-dimensional liquid* portion $A_L(t)$ (see Figure 3.14). For this purpose one has to normalise the amplitudes of both functions: $V(t)/V(0)$ and $A_L(t)/A_I$ (Figure 3.16).

This representation shows a clear functional correlation between the classically obtained time dependence of liquid foam volume fraction and the optically determined time dependence of the two-dimensional liquid portion of the foam.

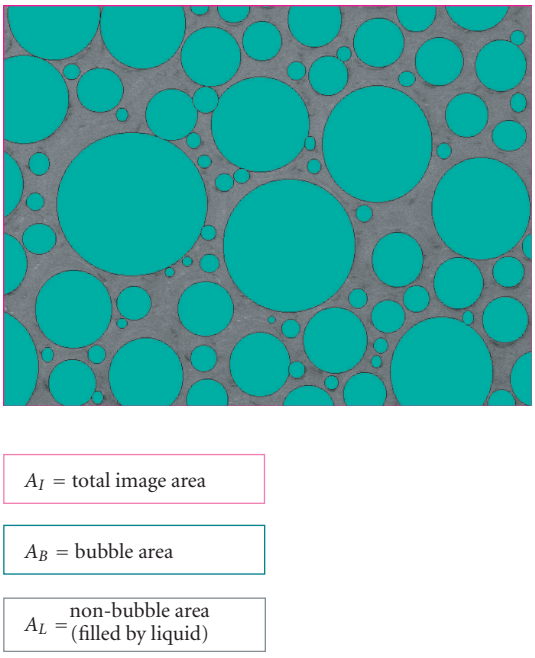

Figure 3.13. Determination of the liquid fraction of foam from a foam image taken as snapshot of shrinking beer foam with trapped bubbles areas.

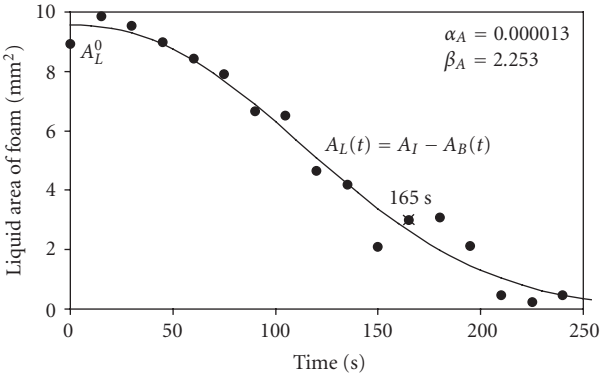

Figure 3.14. Temporal development of the *two-dimensional liquid area* of the foam pictures according to (3.14). For the marked point at 165 s, see Figure 3.15.

3.5. Bubble size distribution. Usually, foam is characterised by its bubble size distribution function. Starting with a very narrow distribution function (Figure 3.17) immediately after the ultrasound treatment of the beer sample, we observed a fast broadening

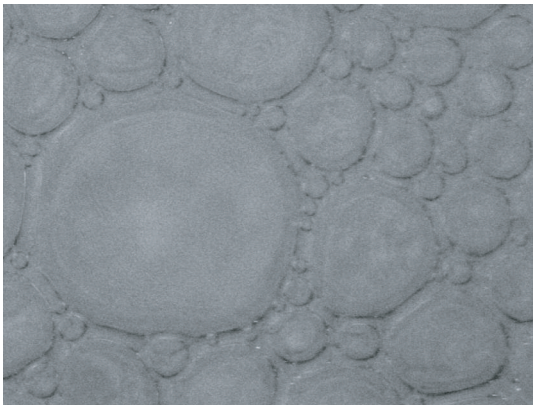

Figure 3.15. Snapshot of the *two-dimensional* arrangement of the bubbles at the inner walls of the glass after 165 s.

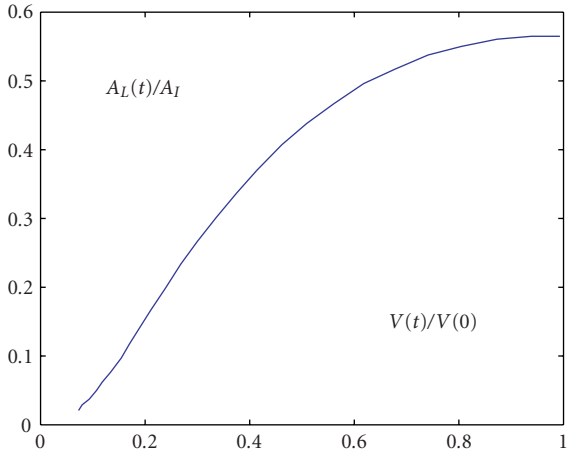

Figure 3.16. Correlation between the normalised two-dimensional liquid foam area and the three-dimensional liquid foam volume fraction. The process starts in the upper right corner.

during the initial state *I* of drainage due to ordinary diffusion (Figure 3.18(a)). But in the consolidation stage *C* we observed a very surprising behaviour. Instead of continuing the normal diffusion process, the distribution function splits into many separated peaks (Figure 3.18(b)). Only very few and quite different bubble sizes survived.

This very strange behaviour encouraged us to look for another method of description for the development of the temporal size distribution function. Starting from the famous articles of Ruch on *diagram lattices as structural principle* [23] on *the principles of increasing mixing* [25] and on *information extent and information distance* [24] we suggest a model for bubble size distribution described in the following section.

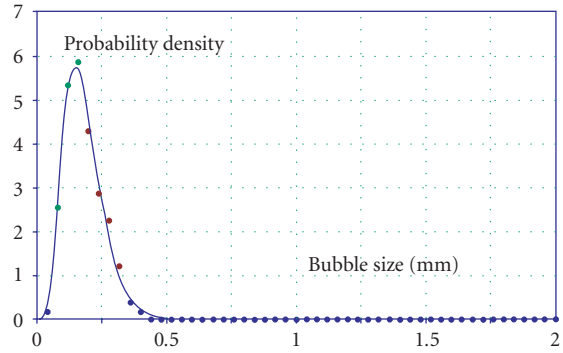

Figure 3.17. Bubble size distribution function (immediately after foaming up, $t \approx 0$ s); the probability density is shown as a function of the bubble sizes.

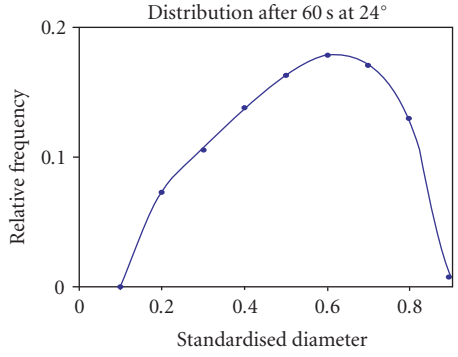

(a)

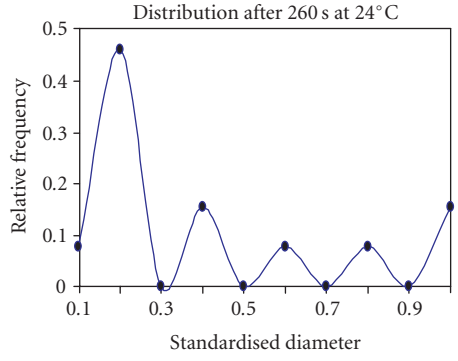

(b)

Figure 3.18. Bubble size distribution functions: (a) 60 s and (b) 260 s after foaming up at 24° C; the relative frequency is shown as a function of the bubble size diameters.

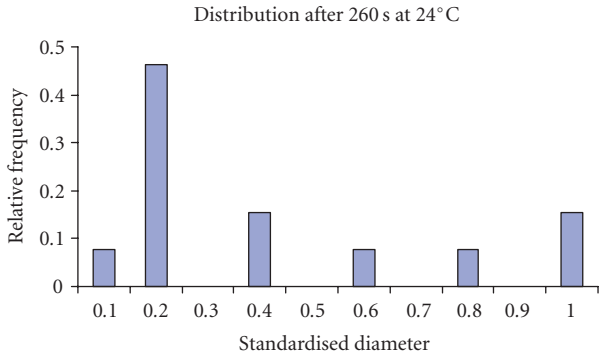

Figure 4.1. Histogram of the bubble size distribution which corresponds to the distribution function 260 s after foaming up which is shown in Figure 3.18(b).

Figure 4.2. A *Young diagram* as a row of $n = 6$ boxes.

4. Diagram lattices and mixing functions as a model for bubble size distributions

Originally Ruch used lattices constructed from *Young diagrams* [26] in order to describe the development of a discrete distribution function. Together with Schönhofer [26] he introduced a *greater* relation for *Young diagrams* [31, 32], in order to answer questions which appear in connection with the theory of chirality functions. This *greater* relation enabled him to construct a lattice. He could show that this lattice introduces a partial order of the *Young diagrams* in contrast to the total order which has been introduced by Young [31]. For describing the time development of irreversible processes in closed systems he mapped the diagrams which are partitions of natural numbers onto the *Shannon entropy* [23, 27]. Going back to Jaynes [12, 13], a comparable idea has been developed at the same time by Uhlmann [29] on the *Shannon entropy* and related functionals on convex sets. Some years later Uhlmann and Alberti described dissipative motions in state space by use of stochastic transformations of convex sets like probability vectors on algebras over real numbers and star algebras like $C^\star$ and $W^\star$ [1].

Surprisingly, this powerful idea of lattices based on *Young diagrams* has later been used to rank biodiversity indices for the comparison of the water quality of lakes [6].

4.1. Histogram representation of bubble size distribution functions and Young diagrams. Now, let us assume that a row with n boxes in a *Young diagram* is a representation of the number, the frequency, or even the probability of bubbles, the size of which belongs to the same interval (see Figures 4.1 and 4.2).

For example, if the diagram consists only of one row (Figure 4.2), then all bubbles belong to the same bubble size interval. This is a realistic assumption for the foam in status

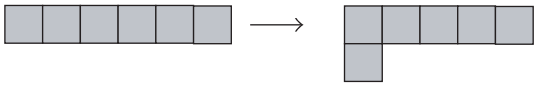

Figure 4.3. Development of a *Young diagram* by shifting one box from the upper row to the next lower row.

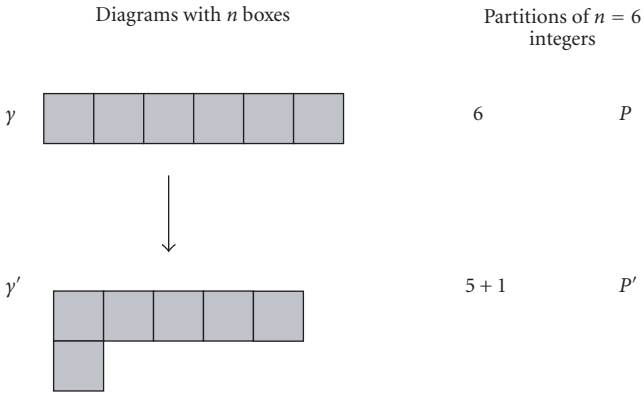

Figure 4.4. Comparison between diagrams γ and γ' with n boxes and their corresponding partitions P and P' of $n = 6$ integers. The unequality relations $\gamma \supset \gamma'$ and $P \supset P'$ hold, respectively.

nascendi immediately after ultrasound treatment (cf. Figure 3.17). During the temporal development, larger bubbles are created, which means in our model that the number of the small initial bubbles diminishes for the benefit of larger bubbles, that is, the diagram develops (see Figure 4.3).

Following the definition of Ruch [23],

> A diagram γ is called greater than a diagram γ', denoted by $\gamma \supset \gamma'$, if γ can be constructed from γ' by moving boxes exclusively upward, that is, from shorter rows into larger or equal ones.

From this definition Ruch transformed a diagram to a smaller neighboured one by moving one box from a larger row into a smaller one.

It is also known [23] that the lengths of the rows of a diagram represent a partition of the integer n, that is, the decomposition of n into a sum of integers. In this case, the definition for the *greater* relation given by Ruch [23] is the following:

> A partition is called greater than another, if the transition from a smaller to the greater one can be made in steps, whereby partition numbers increase at the expense of others which are not larger (see Figure 4.4).

For further details the reader is kindly requested to look at the original literature [23, 26].

Following Ruch's rule for the construction of his *partition lattice* or *diagram lattice*, the most striking result of the *greater* relation is the fact that one gets a total order on

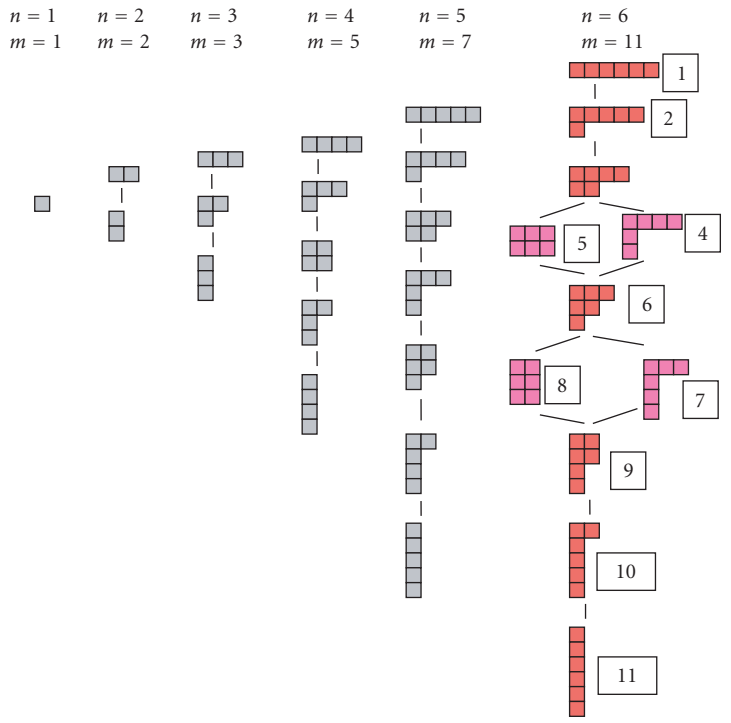

Figure 4.5. Diagram lattices of n boxes and m diagrams within each lattice. The totally ordered sets are given in grey coloured boxes, whereas the partially ordered set for $n = 6$ is represented with red and pink coloured boxes. The pink coloured diagrams of the same level are incomparable elements of this lattice. The numbers p with $1 \le p \le m$ at the right side of the diagrams demonstrate their sequence with respect to the total order given by Young, which is identical with the order of the sums $S(O_\gamma)$ of the partial sums (4.4) [26] in case of the lattice for $n = 6$.

the set of all possible diagrams for n boxes only if $n \le 5$, but a partial order, if $n > 5$ (see Figure 4.5).

The *greater* relation is originally defined [26] by the vector of the partial sums o_i of the ith row of the partition diagram γ, each vector having the length n and filled up with zeros if necessary, for example,

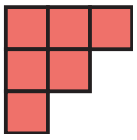

$$\gamma = \begin{pmatrix} \nu_1 \\ \nu_2 \\ \nu_3 \\ \nu_4 \\ \nu_5 \\ \nu_6 \end{pmatrix} = \begin{pmatrix} 3 \\ 2 \\ 1 \\ 0 \\ 0 \\ 0 \end{pmatrix}, \quad O_\gamma = \begin{pmatrix} o_1 \\ o_2 \\ o_3 \\ o_4 \\ o_5 \\ o_6 \end{pmatrix} = \begin{pmatrix} 3 \\ 5 \\ 6 \\ 6 \\ 6 \\ 6 \end{pmatrix}, \quad \text{with} \quad \begin{aligned} o_1 &= \nu_1 \\ o_2 &= \nu_1 + \nu_2 \\ o_3 &= \nu_1 + \nu_2 + \nu_3 \\ o_4 &= \nu_1 + \nu_2 + \nu_3 + \nu_4 \\ &\cdots \end{aligned} \quad . \tag{4.1}$$

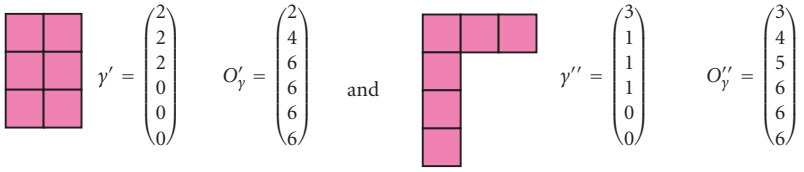

Figure 4.6. Two incomparable *diagrams* (see Figure 4.5 for $n = 6$) are shown together with their correlated partition vectors γ' and γ'' and the vectors O'_γ and O''_γ of the corresponding partial sums.

A partition γ is *greater* than a partition γ', denoted by $\gamma' \subset \gamma$, if and only if

$$o'_i \leq o_i \quad \forall\, i = 1,\ldots,n, \tag{4.2}$$

where n is given by the total number of all boxes of the diagram.

We demonstrate this statement by a comparison of the above-mentioned diagram γ with two other incomparable diagrams (see Figure 4.6).

A simple inspection of these examples shows that the diagrams γ' and γ'' (Figure 4.6) are both smaller than the diagram γ (4.1), that is, $\gamma', \gamma'' \subset \gamma$.

But if we compare both the diagrams γ' and γ'' (Figure 4.6) with each other, we cannot say that γ' is smaller than γ'' nor that the opposite is true since the components of the vectors of the partial sums do not fulfil the condition $o'_i \leq o''_i$ for all $i = 1,\ldots,n$ or its negation, respectively. For this reason the diagrams γ' and γ'' are not comparable.

Some additional statements should be mentioned. One can define a distance $d_i(\gamma,\gamma')$ between two neighboured diagrams γ and γ' as the number of rows which a box has to be shifted in order to step from the upper row of the initial diagram γ to the lower row of the destination diagram γ'. The sum of all distances on a way from the greatest diagram in the diagram lattice consisting of only one row with n boxes to the smallest diagram which contains always one box in each of the n rows is given by the expression (4.3)

$$\sum_{i=1}^{n} d_i(\gamma,\gamma') = \sum_{i=1}^{n-1} i. \tag{4.3}$$

It is remarkable that this sum of distances does not depend on the way from top to bottom, that is, the chosen prejudice of how to step through the incomparable diagrams of the partially ordered lattice does not affect this sum.

The second remark concerns the sum $S(O_\gamma)$ of the partial sums of elements in the vector O_γ of the partial sums. The set of these sums

$$S(O_\gamma) = \sum_{i=1}^{n} o_i \tag{4.4}$$

reflects the structure of the partially ordered set of diagrams. In the case of diagrams with $n < 7$, incomparable elements are characterised by the same number $S(O_\gamma) = S(O'_\gamma)$. Then, we can define that a diagram γ is called *greater* than a diagram γ', if the inequality

Table 4.1. Iterative calculations for the number m of *Young diagrams* for a given number n of boxes.

m	1	2	3	5	7	11	15	22	30	42	56	77	101	135	176	231
n	1	2	3	4	5	6	7	8	9	10	11	12	13	14	15	16
$n-0$	1	1	1	1	1	1	1	1	1	1	1	1	1	1	1	1
$n-1$		1	1	1	1	1	1	1	1	1	1	1	1	1	1	1
$n-2$			1	2	2	2	2	2	2	2	2	2	2	2	2	2
$n-3$				1	2	3	3	3	3	3	3	3	3	3	3	3
$n-4$					1	3	4	5	5	5	5	5	5	5	5	5
$n-5$						1	3	5	6	7	7	7	7	7	7	7
$n-6$							1	4	7	9	10	11	11	11	11	11
$n-7$								1	4	8	11	13	14	15	15	15
$n-8$									1	5	10	15	18	20	21	22
$n-9$										1	5	12	18	23	26	28
$n-10$											1	6	14	23	30	35
$n-11$												1	6	16	27	37
$n-12$													1	7	19	34
$n-13$														1	7	21
$n-14$															1	8
$n-15$																1

The row $n-7$ can be calculated from the sums of $n=7$.

(4.5) between the sum of partial sums (partitionings) holds:

$$S(O_\gamma) > S(O'_\gamma). \tag{4.5}$$

This definition defines a total order onto the set of all diagrams. So, we can enumerate the diagrams in a *natural* way by integers $1 \le p \le m$; $p, m \in \aleph$, where m is the number of diagrams or partitions which can be constructed from n boxes or from the integer n (see Figure 4.5). But there is no polynomial expression to calculate the value m for a given number n, since this problem is a *nonpolynomial NP-complete problem* [9].

However, one can find iteration equations [30] which give the value m for each natural number n of boxes (see Table 4.1 for $n = 1,\ldots,16$). A solution of this problem was presented by Rademacher using a series expansion [21].

4.2. Mapping Young diagrams on scalar functions. If one normalises the number of boxes $\nu_{\gamma,i}$ in the ith row of a given *Young diagram* $\gamma = (\nu_{\gamma,1}, \nu_{\gamma,2}, \ldots, \nu_{\gamma,i}, \ldots, \nu_{\gamma,n})$ of n boxes (or the corresponding partition) with respect to the overall number of boxes n according to (4.6),

$$p_{\gamma,i} = \frac{\nu_{\gamma,i}}{n}, \tag{4.6}$$

one can map all diagrams onto a scalar function, for example, the *Shannon entropy* $I(\gamma)$ [23, 27]:

$$I(\gamma) = F_1(\gamma) = -\sum_{i=1}^{n} p_{\gamma,i} \mathrm{ld}(p_{\gamma,i}). \tag{4.7}$$

By this way one introduces a total order on the set of all *Young diagrams* belonging to a given number n of boxes.

On the other hand, one can also obtain a total order $\gamma \geq \gamma'$ on the set of diagrams or partitions for any given number n by the definition [26]:

> $\gamma > \gamma'$, if moving from top to bottom in the diagram lattice by comparison of corresponding rows the first row is reached, where the relation $\nu_i > \nu_i'$ holds.

This definition by Ruch and Schönhofer [26] of a total order on the set of diagrams corresponds in the case of $n < 7$ to the total order which is given by the sum $S(O_\gamma)$ (4.4) of partial sums.

Figure 4.7 shows (a) the *Shannon entropies* of the diagrams as a function of the consecutive numbers p of the totally ordered set of entropy values, and (b) the corresponding partial sums of *Shannon entropies* up to p. Both functions are increasing monotonous and discrete functions of the ordering numbers p of the diagrams which correlate with the progression of the diffusion process.

For the further discussion let us mention that the sum S of all normalised row values $p_{\gamma,i}$ (4.6) of a partition vector γ is equal to one (simplex condition), that is, the trace of the vector is one,

$$S = \sum_{i=1}^{n} p_{\gamma,i} = 1, \quad 0 \leq p_{\gamma,i} \leq 1. \tag{4.8}$$

By the simplex condition (4.8) one obtains a normalised and bounded domain—the simplex S_n—on which the *Shannon entropy* is defined. Also, the function over this domain of definition itself, that is, the *Shannon entropy* $I(\gamma) = F_1(\gamma)$ (4.7) can be normalised for any number n of boxes by (4.9) (see Figure 4.8 for $n = 3$):

$$F_2(\gamma) = \frac{1}{\mathrm{ld}(n)} F_1(\gamma) = -\frac{1}{\mathrm{ld}(n)} \sum_{i=1}^{n} p_{\gamma,i} \mathrm{ld}\,(p_{\gamma,i}). \tag{4.9}$$

This *normalised Shannon entropy* $F_2(\gamma)$ maps the *Young diagrams* onto real numbers of the closed interval $[0,1]$:

$$\gamma \longmapsto F_2(\gamma) \in [0,1]. \tag{4.10}$$

It is now very important to realise that the function $F_2(\gamma)$ is a *concave* function [19] (also called *convex from the above* [5, 11]) over the simplex S_n which in addition fulfils the restrictions

$$\begin{aligned} F(S_n) &= 0, \quad \text{for } \nu_i = 1,\ \nu_j \neq \nu_i, \\ F(S_n) &= 1, \quad \text{for } \nu_1 = \nu_2 = \cdots = \nu_n = \frac{1}{n}. \end{aligned} \tag{4.11}$$

The *Shannon information entropy* functions $F_1(\gamma)$ or $F_2(\gamma)$, respectively, can be considered as a measure for the gain of information if one executes an experiment where the probabilities of its events are distributed under the restriction of the simplex constraints (4.8).

The *Shannon entropy* is only one possible choice among an infinite number of possibilities to find concave scalar functions over the simplex S_n. Examples for other concave

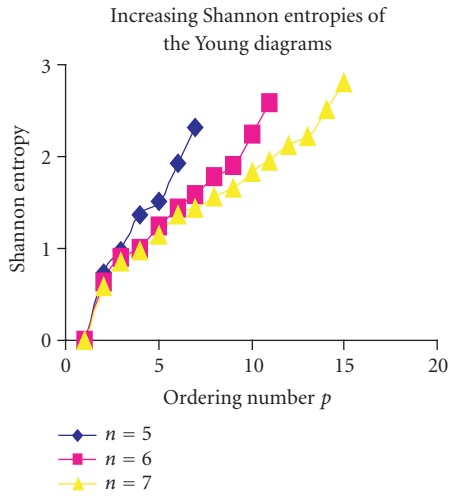

(a)

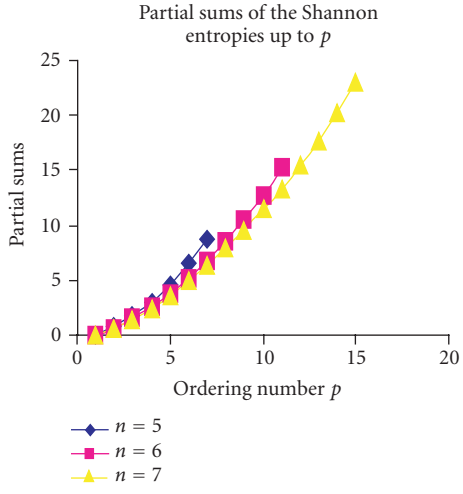

(b)

Figure 4.7. Progression of diffusion process: (a) *Shannon entropies* of the *Young diagrams* as a function of the ordering number p according to (4.4), (b) partial sums of *Shannon entropies* up to p as a function of p.

functions—comparable with the *normalised Shannon entropy* F_2—which map the *Young diagrams* onto the closed interval $[0,1]$ and which fulfil condition (4.11), respectively, over n-dimensional simplices S_n as domains are

(i) the *normalised general tent function* $F_3(\gamma)$ (see Figure 4.9 for $n = 3$),

$$F_3(\gamma) = 1 - \frac{n}{2(n-1)} \sum_{i=1}^{n} \left| p_{\gamma,i} - \frac{1}{n} \right|, \tag{4.12}$$

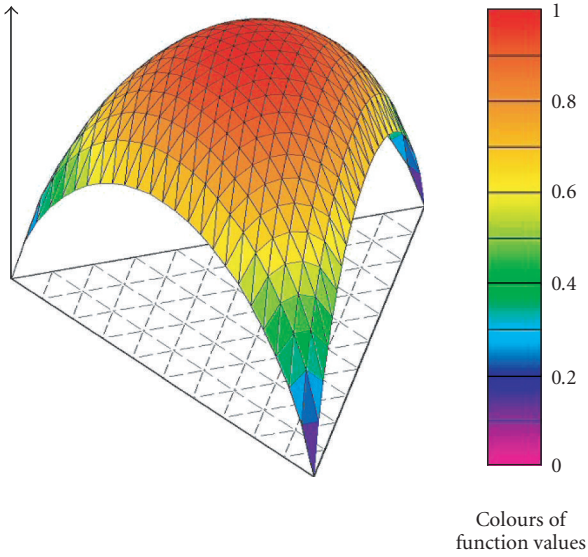

Figure 4.8. *Normalised Shannon entropy* $F_2(\gamma)$ for $n = 3$ defined on the simplex S_2 over triangular coordinates in the plane.

(ii) the *normalised general logistic function* $F_4(\gamma)$,

$$F_4(\gamma) = \frac{n}{n-1} \sum_{i=1}^{n} \left[(1 - p_{\gamma,i})\, p_{\gamma,i} \right], \tag{4.13}$$

(iii) the *normalised general biquadratic function* $F_5(\gamma)$ (stretched to the simplex boundaries, see Figure 4.10 for $n = 3$),

$$F_5(\gamma) = 1 - \frac{n^4}{(n-1)^4 + (n-1)} \sum_{i=1}^{n} \left(p_{\gamma,i} - \frac{1}{n} \right)^4, \tag{4.14}$$

(iv) the *normalised general k-quadratic function* $F_6(\gamma)$ (stretched to the simplex boundaries), which becomes the logistic function for $k = 1$ and the biquadratic function for $k = 2$, respectively,

$$F_6(\gamma) = 1 - \frac{n^{2k}}{(n-1)^{2k} + (n-1)} \sum_{i=1}^{n} \left(p_{\gamma,i} - \frac{1}{n} \right)^{2k}, \quad \text{with } k = 1,2,\ldots. \tag{4.15}$$

There are further functions fulfilling condition (4.11) over n-dimensional simplices S_n, such as

(i) the *normalised general biquadratic function* $F_7(\gamma)$ (*delta-like* compressed to the centre of simplex),

$$F_7(\gamma) = \frac{n^3}{(n-1)^2} \sum_{i=1}^{n} (1 - p_{\gamma,i})^2 p_{\gamma,i}^2, \tag{4.16}$$

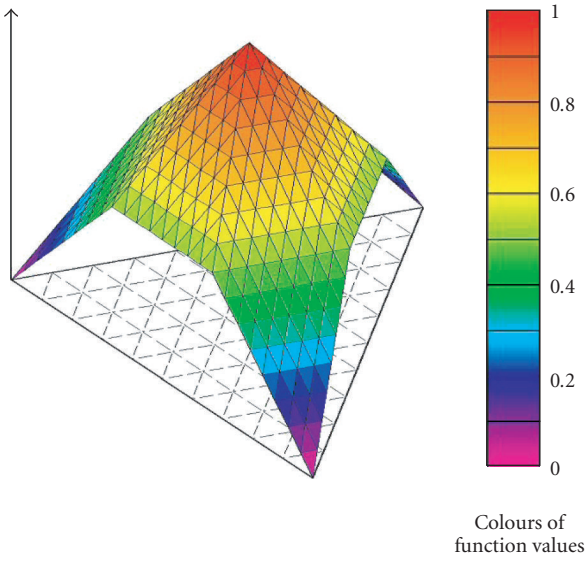

Figure 4.9. *Normalised tent function* $F_3(\gamma)$ for $n = 3$ defined on the simplex S_2 over triangular coordinates in the plane.

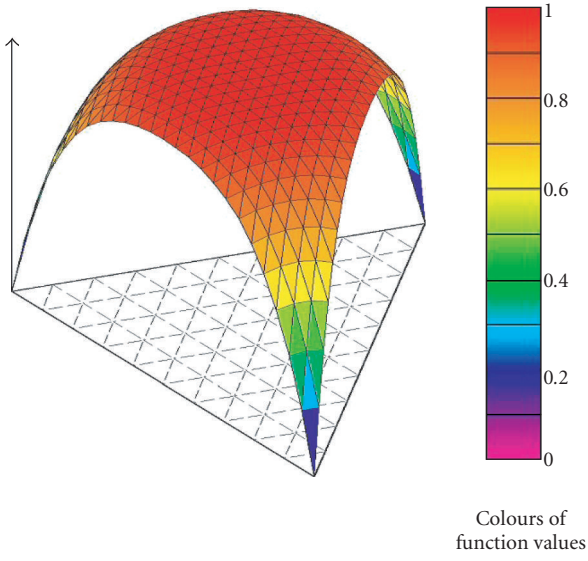

Figure 4.10. *Normalised biquadratic function* $F_5(\gamma)$ for $n = 3$ defined on the simplex S_2 over triangular coordinates in the plane.

(ii) the *normalised general k-quadratic function* $F_8(\gamma)$ (*delta-like* compressed to the centre of simplex, see Figure 4.11 for $n = 3$ and $k = 4$), which becomes the logistic

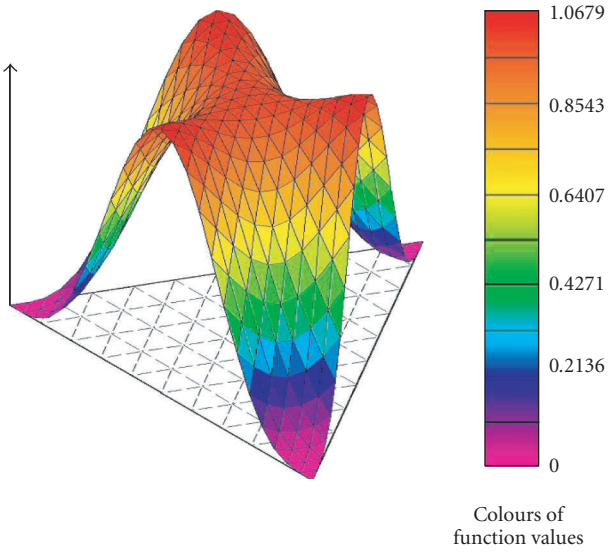

Figure 4.11. *Normalised k-quadratic delta-function* $F_8(\gamma)$ for $n = 3$ and $k = 4$ defined over triangular coordinates in the plane.

function for $k = 1$ and the biquadratic function for $k = 2$, respectively,

$$F_8(\gamma) = \frac{n^{2k-1}}{(n-1)^k} \sum_{i=1}^{n} \left(1 - p_{\gamma,i}\right)^k p_{\gamma,i}^k, \quad \text{with } k = 1,2,\ldots. \tag{4.17}$$

Both functions are not concave over the whole simplex, on which they are defined (see Figure 4.11), although they fulfil condition (4.11), that is, they are symmetric to the centre of equally distributed values $p_{\gamma,i} = 1/n$ with function value one, and they take the function value zero if one $p_{\gamma,i}$ gets 1 and all other $p_{\gamma,j}$ vanish; but their mapping interval exceeds the value 1 in general.

A nonpolynomial type of concave functions fulfilling condition (4.11) which maps the *Young diagrams* onto the closed interval $[0,1]$ over n-dimensional simplices S_n as well is given by the *normalised general product of trigonometric functions* $F_9(\gamma)$:

$$F_9(\gamma) = \frac{1}{n\cos(\pi/2n)\sin(\pi/2n)} \sum_{i=1}^{n} \cos\left(p_{\gamma,i}\right) \sin\left(p_{\gamma,i}\right). \tag{4.18}$$

The representations of functions $F_2(\gamma)$, $F_3(\gamma)$, $F_5(\gamma)$, and $F_8(\gamma)$ in Figure 4.8 to Figure 4.11 on the S_2 simplex over triangular coordinates were chosen to give an intuitive insight into these types of functions on higher simplices S_i with $i > 1$. Recall that a *Young diagram* γ of n boxes corresponds always to a simplex S_{n-1} with n vertices defining the domain of the functions $F_i(\gamma)$. In fact, our application leads to functions over much higher simplices which cannot be drawn easily in a three-dimensional graphical representation.

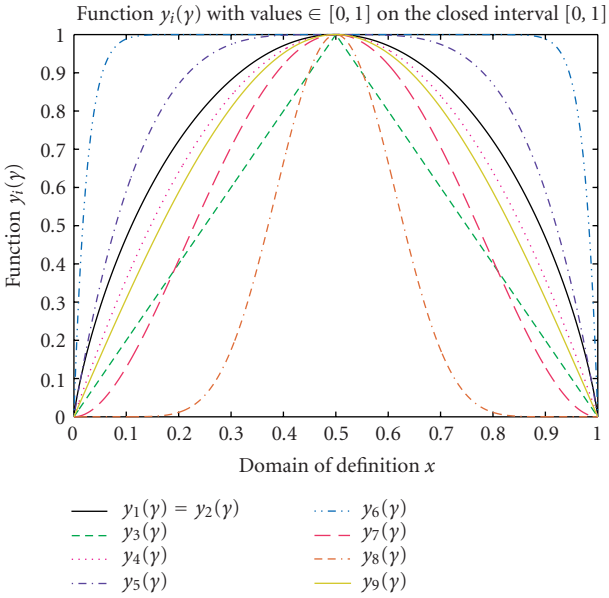

Figure 4.12. Comparison of the normalised functions $y_1,\ldots,y_9$ on the simplex S_1, that is, the closed interval $[0,1]$.

The functions $F_1(\gamma)$ to $F_6(\gamma)$ as well as $F_9(\gamma)$ are concave functions on the simplex S_i, that is, the following equation [19]:

$$\frac{f(x_1)+f(x_2)}{2} < f\left(\frac{x_1+x_2}{2}\right) \tag{4.19}$$

holds for any variable x_i with $i = 1,2$ (x_i should be identified with $p_{\gamma,i}$ in our context). On the other hand, the functions F_7 and F_8 are neither concave nor convex over the whole simplex (see Figure 4.11), but it is remarkable that both functions exhibit several maxima although they are normalised to 1 in the centre of the simplex where all variables have equally distributed values x_i, for example, $x_1 = x_2 = x_3 = 1/3$ in case of the simplex S_2. This kind of functions could be of interest with respect to structure formations in processes far away from equilibrium and will be discussed in greater detail in Section 4.5.

4.3. Scalar functions on the simplex S_1. Figure 4.12 shows a comparison of the scalar functions $y_1 \equiv F_1(\gamma)$ to $y_9 \equiv F_9(\gamma)$ defined in the previous section for the special case of the well known simplex S_1, that is, the closed interval $[0,1]$. The choice of the S_1 simplex means that we consider only two variables or a *Young diagram* of only $n = 2$ boxes, respectively, where the simplex condition of the domain of definition is given by

$$x_1 + x_2 = 1 \quad \text{or} \quad x \equiv x_1 = 1 - x_2, \quad 0 \le x_i \le 1. \tag{4.20}$$

Under these assumptions the *Shannon entropy functions* $F_1(\gamma)$ (4.7) and $F_2(\gamma)$ (4.9) take the form

$$y_1 = y_2 = -[x_1 \operatorname{ld} x_1 + x_2 \operatorname{ld} x_2] = -[x \operatorname{ld} x + (1-x) \operatorname{ld}(1-x)]. \tag{4.21}$$

The *tent function* $F_3(\gamma)$ (4.12) transforms to y_3 according to (4.22). Note that y_3 is an *affine* function [19] since it is concave (convex from the above) and convex (convex from the below) simultaneously.

$$y_3 = 1 - 2|x - 0.5|. \tag{4.22}$$

The *logistic function* $F_4(\gamma)$ (4.13) gets the well-known shape

$$y_4 = 1 - 4(x-0.5)^2 = 2^2 x(1-x). \tag{4.23}$$

The *general biquadratic function* $F_5(\gamma)$ (4.14) and the *k-quadratic function* $F_6(\gamma)$ (4.15) which are stretched to the simplex boundaries change into

$$\begin{gathered} y_5 = 1 - 2^4 (x-0.5)^4, \\ y_6 = 1 - 2^k (x-0.5)^k, \quad \text{e.g., } y_6 = 1 - 2^{20}(x-0.5)^{20} \quad \text{for } k = 10, \end{gathered} \tag{4.24}$$

respectively. For $k \to \infty$, the function y_6 tends to the *quadratic pulse-function H of width one* given by (4.25):

$$H = \begin{cases} 1, & \text{for } 0 < x_i < 1, \\ 0, & \text{otherwise.} \end{cases} \tag{4.25}$$

The *product function of trigonometric functions* $F_9(\gamma)$ (4.18) which is also concave but of nonpolynomial type becomes

$$y_9 = 2 \sin\left(\frac{\pi}{2} x\right) \cos\left(\frac{\pi}{2} x\right). \tag{4.26}$$

The *general biquadratic function* $F_7(\gamma)$ (4.16) and the *k-quadratic function* $F_8(\gamma)$ (4.17) both of which are *delta-like* compressed to the centre of simplex take now the simple forms

$$\begin{gathered} y_7 = 2^4 x^2 (1-x)^2, \\ y_8 = 2^k x^k (1-x)^k, \quad \text{e.g., } y_8 = 2^{20} x^{10} (1-x)^{10} \quad \text{for } k = 10, \end{gathered} \tag{4.27}$$

respectively. Both these functions y_7 and y_8 reflect the fact that they are neither concave nor convex over the whole closed interval $[0,1]$. But they have a maximum at $x_1 = x_2 = 1/2$ in contrast to their corresponding functions $F_7(\gamma)$ and $F_8(\gamma)$ defined on higher dimensional simplices which in general show a minimum at the centre of the simplex and various maxima symmetrically distributed around this point.

All these functions can be used as measures characterising the disorder or mixing of the system under inspection. We call the functions $F_1(\gamma)$ to $F_6(\gamma)$ and $F_9(\gamma)$ or the functions

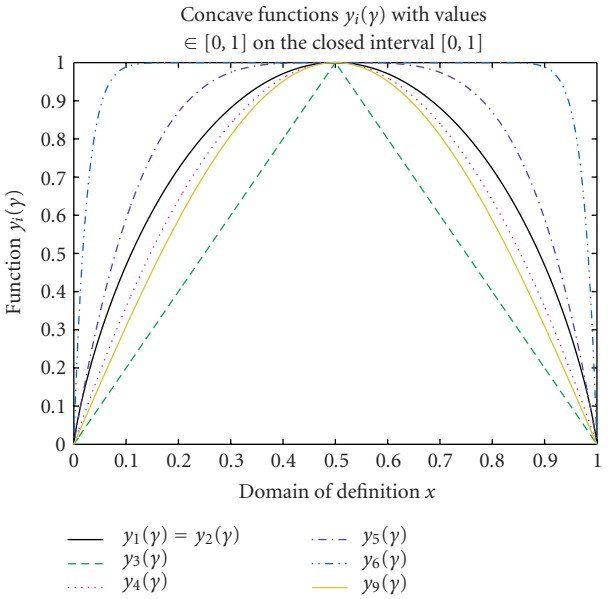

Figure 4.13. Comparison of the normalised concave *entropy-like mixing functions* $y_1, \ldots, y_6$ and y_9 on the simplex S_1, that is, the closed interval $[0,1]$. The *tent function* y_3 is an affine function, since it is concave and convex simultaneously.

y_1 to y_6 and y_9, respectively, *entropy-like mixing functions* (see Figure 4.13), since they form a family of concave functions on the interval $[0,1]$ the maxima of which are 1 in case of $x_i = 1/n$ for all indices i.

4.4. Ordering of mixing functions in higher dimensional diagram lattices. However, depending on our choice of the *entropy-like mixing function* the sequences of the diagrams change, which can easily be seen from the occurrence of extreme values if one compares the entropy like mixing functions with each other (Figure 4.14).

The partially ordered lattice of the diagrams describes the system without prejudice for choosing a way from top to bottom in the lattice, that is, from order to disorder. The classical *Shannon entropy* is by no means a unique choice to measure disorder or order, respectively. The choice of a special *entropy-like mixing function* is nothing else than the introduction of a prejudice concerning a special mapping by a mixing function of the diagrams or the corresponding partitions onto the interval $[0,1]$. The projection may change the sequence of steps from top to bottom in the lattice, that is, the sequence of states on the way from order to disorder. For example, if one takes the biquadratic $F_5(\gamma)$ (4.14) of the diagrams with $n = 6$ boxes as a function of the correlated *Shannon entropy* $F_2(\gamma)$, the incomparable diagrams of the pairs γ_4 and γ_5 as well as γ_7 and γ_8, respectively, permute with each other in their sequence (see also Figures 4.5 and 4.14). The sequences of those diagrams which are comparable do not switch their sequence when choosing another partition function than the *Shannon entropy* (see Figure 4.15).

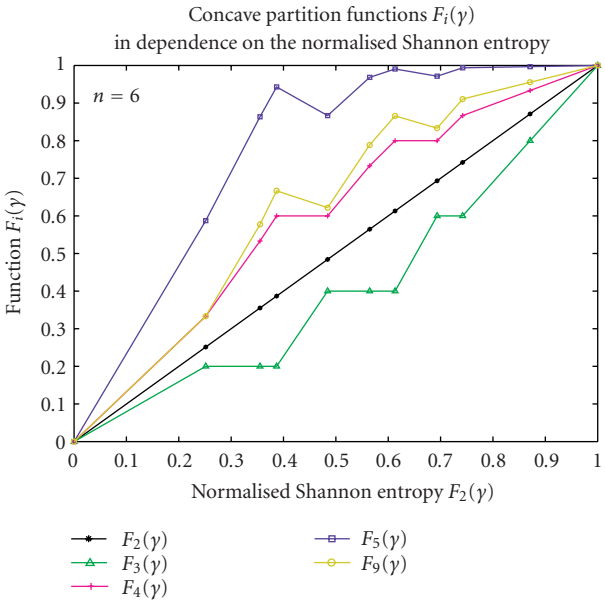

Figure 4.14. Dependence of concave partition functions $F_i(\gamma)$ on the *normalised Shannon entropy* of the *Young diagrams* in case of $n = 6$.

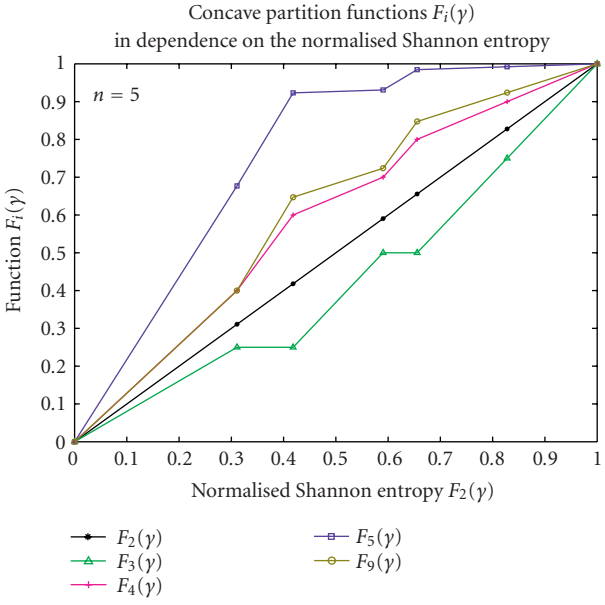

Figure 4.15. Dependence of concave partition functions $F_i(\gamma)$ on the normalised *Shannon entropy* of the *Young diagrams* in case of $n = 5$.

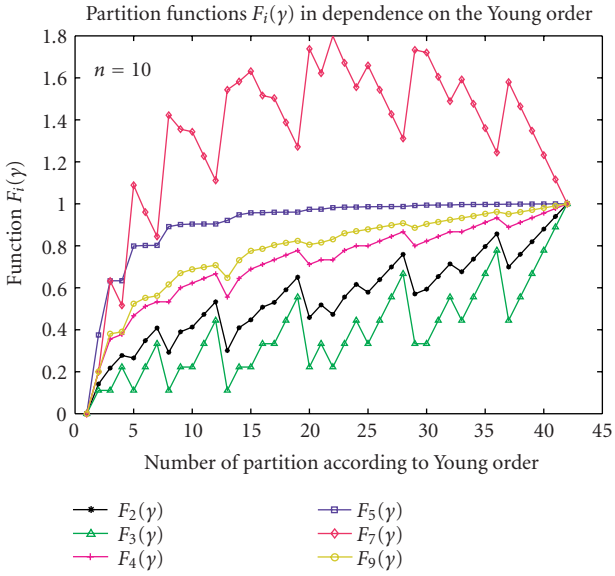

Figure 4.16. Dependence of partition functions $F_i(\gamma)$ on the *Young order* of partial sums for the *Young diagrams* in case of $n = 10$.

As can be seen from Figure 4.16 there is no unique system to select a total order which is preferred with respect to all other choices which can be made. The *Young order* is comparable to all the other possibilities forming a total order on the partially ordered lattice of diagrams. But from Figure 4.16 one can see clearly that the set of all *entropy-like mixing functions* forms a family of functions which tends to reflect the *Young order* and that the *k-quadratic functions* $F_6(\gamma)$ (4.15) which are stretched to the simplex boundaries correspond strictly to the *Young order* for the limiting case with $k \to \infty$; and even the biquadratic function $F_6(\gamma)$ (4.14) reproduces the *Young order* exactly up to $n = 13$.

4.5. Nonentropy-like mixing functions. In contrast to the concave *entropy-like mixing functions* discussed above, the functions y_7 and y_8 or—more generally—$F_7(\gamma)$ and $F_8(\gamma)$, respectively, which are not concave over the whole simplex of their definition, show the following remarkable properties.

(1) In case of S_1 or the closed interval $[0,1]$ as domain of definition, y_7 and y_8 are concave around the centre of S_1 at $x = 0.5$ and convex (from the below) towards the boundaries at $x = 0$ and $x = 1$, respectively (see Figure 4.12). In other words, they have two crossing points with the *affine tent function* y_3 symmetrically arranged with respect to the centre of S_1 both of them moving to $x = 0.5$ for $k \to \infty$. As a consequence, only in the region around $x = 0.5$, that is, in case of highly disordered systems (close to equilibrium or almost equally distributed), y_7 and y_8 behave as *entropy-like mixing functions,* yielding a high increase of information if one executes an experiment. But beyond the crossing points with the *affine tent function* y_3—that is, on the convex sides—they rapidly tend to zero. If one now

takes into account that only at the vertices of the simplex the uncertainty of an experiment is zero or—equivalently—the knowledge is maximal (complete), one can conclude that in case of these non-overall concave functions even at comparably less knowledge the additional gain in information is very small.

(2) As can be seen exemplarily from Figure 4.11 the functions $F_7(\gamma)$ and $F_8(\gamma)$ defined on higher simplices S_i with $i > 1$ show in general a minimum at the centre of the simplex and various maxima symmetrically distributed around this point; hence they exhibit function values greater than one (see Figure 4.16, red polygon) if they are normalised to 1 for an equilibrated or equally distributed system corresponding to the *Young diagram* with the highest number m of the correlated *Young order*. As a consequence, they have convex (from the below) regions not only over the vicinities of the simplex vertices but also a convex area over the centre of the simplex and concave parts symmetrically arranged with respect to the simplex centre.

If one interprets this behaviour of functions $F_7(\gamma)$ and $F_8(\gamma)$ in terms of statements about information content, an experiment in the immediate neighbourhood the equilibrated or equally distributed system does not lead to the maximum gain of information, although there is maximum uncertainty and—as a consequence—the least known knowledge. On the other hand, somewhat farther away from the equilibrium point there are several (equivalent) situations with maximum increase of information, but already some knowledge. The consequences from the function behaviour in convex regions on the simplex corners are the same as described above for y_7 and y_8.

Considering these interesting properties we suggest—with the necessary caution—that the functions $F_7(\gamma)$ and $F_8(\gamma)$ may be of interest for the description of dynamically fluctuating systems and the explanation of structure formations in processes.

5. Conclusion

It was our aim to characterise the decay of beer foam by quite different methods like measuring the temporal behaviour of the foam volume, the fractal dimension of the two-dimensional photographs, of the bubble arrangements, the estimation of liquid content in the foam phase, and the bubble size distribution functions. It is our finding that the foam volume does not shrink simple exponentially but in terms of higher order according to the equation $\ln V(t) = a - bt - ct^{2.5}$ (3.1).

The term $ct^{2.5}$ describes the reorganisation of the bubble arrangements which will lead to an Apollonian gasket of bubbles. This process could be described by the fractal dimension of the correlated bubble pictures and tends to the fractal dimension $D \approx 1.3058$ [3] of the Apollonian packages of circles. Both methods have a great potential of industrial and environmental application, since they allow to follow the decay of foams easily. This could be demonstrated via the estimation of the actual fluid part remaining in the foam during its decay.

The bubble size distribution function of led to the question how to compare different bubble size distribution diagrams. Following the idea of Ruch [23], we described the bubble size diagrams by *Young diagrams* forming a partially ordered lattice. The temporal

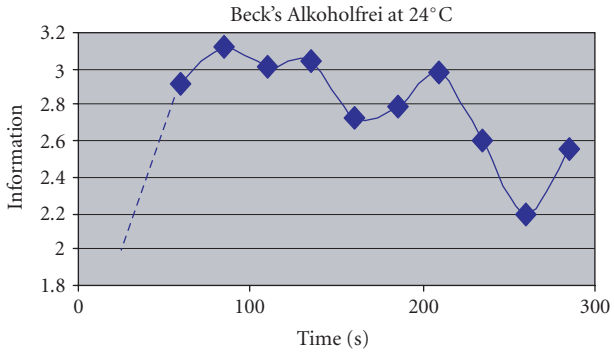

Figure 5.1. The *Shannon information entropy* of the bubble size distribution of *Beck's Alkoholfrei* beer at 24° C as a function of time.

sequence of *Young diagrams* reflects the movement of a closed system towards its equilibrium attractor. Mapping the *Young diagrams* on scalar functions, for example, the *Shannon entropy*, one can follow the temporal development of the system by its correlated *Shannon entropy* or information content, respectively (Figure 5.1).

It was our expectation to find a smooth, monotonously growing information function in dependence on time. Surprisingly we got an oscillating behaviour of this information function for 0° C, 8° C, and 24° C, respectively. This can be understood qualitatively if we take into consideration that our system is by no means a closed system and, as a consequence, one should be able to observe structure formation processes during time intervals of its development. On the other hand, we started with a very narrow bubble size distribution function immediately after the ultrasound degassing of the beer, where one should expect classically a broadening of this distribution function and an increase of the information entropy, but not the occurrence of a multimodal distribution function oscillatory swinging up and down.

To get an insight into all these problems we investigated the behaviour of different mixing functions mapped on the simplex S_n which is correlated to a lattice of *Young diagrams* with n boxes. There is an infinite number of concave functions which can be used to characterise the mixing of states or bubble sizes, respectively, which is described by one *Young diagram*. But any choice of a special function out of this set of concave functions corresponds to the introduction of a prejudice with respect to the definition of a total order on the partial order of the lattice of *Young diagrams* with n boxes. Therefore, we concluded that not only one function, but the total set of all concave functions which are *entropy-like mixing functions* is an appropriate, unprejudiced measure for the mixing of states or bubbles, respectively. In addition, we suggested that the *nonentropy-like mixing functions* may be an adequate description for structure formations in processes.

Obviously, the decay of beer foam is finished before reaching the equilibrium—which of course can never be reached. Before vanishing totally, the foam system remains in a state which can roughly be described by distribution functions belonging to states anywhere in the middle of a partially ordered lattice of *Young diagrams* of many boxes. It will be the task of our next work to describe the oscillating movement of the foam system into

this region based on an analysis of the doubly stochastic matrices which transform the vectors of the bubble size distribution functions during their temporal development into each other.

Acknowledgments

We gratefully acknowledge many stimulating discussions with E. Swart. Also we wish to thank U. Sydow for helpful proofreading of this article. Parts of this article have already been reported by S. Sauerbrei and P. Plath in discussions on the Winterseminar at Zeinisjoch (March 13th, 2004) and at Kruess company (Hamburg; June 25th, 2003).

References

[1] P. M. Alberti and A. Uhlmann, *Dissipative Motion in State Spaces*, Teubner-Texte zur Mathematik, vol. 33, BSB B. G. Teubner, Leipzig, 1981.
[2] J. J. Bikerman, *Foams*, Springer, New York, 1973.
[3] D. W. Boyd, *Improved bounds for the disk-packing constant*, Aequationes Mathematicae **9** (1973), no. 1, 99–106.
[4] ———, *The residual set dimension of the Apollonian packing*, Mathematika **20** (1973), 170–174.
[5] I. N. Bronšteĭn and K. A. Semendjajew, *Taschenbuch der Mathematik*, 20th ed., Nauka, Moscow; BSB B. G. Teubner, Leipzig, 1981.
[6] R. Brüggemann, N. Walz, M. Brauns, and W. Ostendorp, *Beitragsserie: Seeufer, ein vergessenes Ökoton, Beitrag 3*, UWST- Z. Umweltchemie Ökotox **16** (2004), no. 1, 48–56.
[7] L. Burmester, *Geometrische Untersuchung der Theorie der Bewegung des Grundwassers im Gerölle und der Wasserfilterung durch Sand*, Zeitschrift für Angewandte Mathematik und Mechanik **4** (1924), no. 1, 33–52.
[8] C. J. Dale, S. G. Walker, and A. Lyddiatt, *Dynamic changes in the composition and physical behaviour of dispensed beer foam*, Journal of the Institute of Brewing **99** (1993), 461–466.
[9] L. Goldschlager and A. Lister, *Informatik—Eine moderne Einführung*, Carl Hanser, München, 1984.
[10] E. C. Haß, R. Ottensmeyer, and A. Wittstock, *Schaumcharakterisierung mit optischen Messtechniken und PC-gestützter Bildverarbeitung*, tm—Technisches Messen **71** (2004), no. 11, 603–612 (German).
[11] A. M. Jaglom and I. M. Jaglom, *Wahrscheinlichkeit und Information*, 4th ed., VEB Deutscher Verlag der Wissenschaften, Berlin, 1984.
[12] E. T. Jaynes, *Information theory and statistical mechanics*, Physical Review **106** (1957), no. 4, 620–630.
[13] ———, *Information theory and statistical mechanics. II*, Physical Review **108** (1957), no. 2, 171–190.
[14] A. Leike, *Demonstration of the exponential decay law using beer froth*, European Journal of Physics **23** (2002), no. 1, 21–26.
[15] B. B. Mandelbrot, *Fractals: Form, Chance, and Dimension*, W. H. Freeman, California, 1977.
[16] ———, *The Fractal Geometry of Nature*, W. H. Freeman, California, 1982.
[17] ———, *Die fraktale Geometrie der Natur*, Akademie, Berlin, 1987.
[18] E. Manegold, *Kapillarsysteme. Bd. 1*, Straßenbau, Chemie und Technik Verlagsgesellschaft mbH, Heidelberg, 1955.
[19] H. Meschkowski, *Mathematisches Begriffswörterbuch*, BI- Hochschultaschenbücher 99/99a, Bibliographisches Institut, Mannheim, 1965.
[20] Ch. Pöppe, *Kreispackungen*, Spektrum der Wissenschaften **November** (2002), 116–118.

[21] H. Rademacher, *On the partition function $p(n)$*, Proceedings of the London Mathematical Society, Series 2 **43** (1937), 241–254.
[22] T. Rothmann and H. Fukagawa, *Sangaku: Japanische Geometrie*, Spektrum der Wissenschaften **July** (1998), 87–90.
[23] E. Ruch, *The diagram lattice as structural principle*, Theoretica Chimica Acta **38** (1975), no. 3, 167–183.
[24] E. Ruch and B. Lesche, *Information extent and information distance*, The Journal of Chemical Physics **69** (1978), no. 1, 393–401.
[25] E. Ruch and A. Mead, *The principle of increasing mixing character and some of its consequences*, Theoretica Chimica Acta **41** (1976), no. 2, 95–117.
[26] E. Ruch and A. Schönhofer, *Theorie der Chiralitätsfunktionen*, Theoretica Chimica Acta **19** (1970), no. 3, 225–287.
[27] C. E. Shannon, *A mathematical theory of communication*, The Bell System Technical Journal **27** (1948), 379–423 and 623–656.
[28] K. Simonyi, *Kulturgeschichte der Physik*, Urania, Leipzig, 1990.
[29] A. Uhlmann, *On the Shannon entropy and related functionals on convex sets*, Reports on Mathematical Physics **1** (1970), no. 2, 147–159.
[30] E. W. Weisstein, *Partition Function P.*, From *Mathworld—A Wolfram Web Resource*, http://mathworld.wolfram.com/PartitionFunctionP.html.
[31] A. Young, *On quantitative substitutional analysis I*, Proceedings of the London Mathematical Society **33** (1901), 97–146, See also: A. Young, *On Quantitative Substitutional Analysis*, The Collected Papers of Alfred Young 1873–1940, Mathematical Expositions no. 21, University of Toronto Press, Toronto and Buffalo, 1977, pp. 42–91., A. Young, *On Quantitative Substitutional Analysis (Third Paper) (1927)*, The Collected Papers of Alfred Young 1873–1940, Mathematical Expositions no. 21, University of Toronto Press, Toronto and Buffalo, 1977, pp. 352–389.
[32] ———, *The Collected Papers of Alfred Young (1873–1940)*, Mathematical Expositions, no. 21, University of Toronto Press, Ontario, 1977, With a foreword by G. de B. Robinson and a biography by H. W. Turnbull.

S. Sauerbrei: Institut für Angewandte und Physikalische Chemie–Arbeitsgruppe Chemische Synergetik, Universität Bremen, Bibliothekstraße NW 2, 28359 Bremen, Germany
E-mail address: sauerbrei@uni-bremen.de

E. C. Haß: Institut für Angewandte und Physikalische Chemie–Arbeitsgruppe Chemische Synergetik, Universität Bremen, Bibliothekstraße NW 2, 28359 Bremen, Germany
E-mail address: echass@uni-bremen.de

P. J. Plath: Institut für Angewandte und Physikalische Chemie–Arbeitsgruppe Chemische Synergetik, Universität Bremen, Bibliothekstraße NW 2, 28359 Bremen, Germany
E-mail address: plath@uni-bremen.de